Materials and Design 37 (2012) 193–201

Contents lists available at SciVerse ScienceDirect

Materials and Design

journal homepage: www.elsevier.com/locate/matdes

Micromechanical analysis of mechanical heterogeneity effect on the ductile tearing of weldments

B. Younise [a], A. Sedmak [a,*], M. Rakin [b], N. Gubeljak [c], B. Medjo [b], M. Burzić [d], M. Zrilić [b]

[a] Faculty of Mechanical Engineering, University of Belgrade, Kraljice Marije 16, 11120 Belgrade, Serbia
[b] Faculty of Technology and Metallurgy, University of Belgrade, Karnegijeva 4, 11120 Belgrade, Serbia
[c] Faculty of Mechanical Engineering, University of Maribor, Smetanova 17, SI-2000 Maribor, Slovenia
[d] Innovation Center of the Faculty of Mechanical Engineering, Belgrade, Kraljice Marije 16, 11120 Belgrade, Serbia

ARTICLE INFO

Article history:
Received 16 October 2011
Accepted 2 January 2012
Available online 9 January 2012

Keywords:
D. Weldments
E. Mechanical heterogeneity
I. Ductile fracture

ABSTRACT

The objective of this study is determination of the effect of mechanical heterogeneity on ductile crack initiation and propagation in weldments using micromechanical approach. Welded single-edge notched bend (SENB) specimens were experimentally and numerically analysed. Material properties of welded joint zones were estimated using a combined experimental and numerical procedure; strains on a smooth tensile specimen were determined using ARAMIS stereometric measuring system in order to obtain true stress – true strain curves. High-strength low-alloyed steel was used as base metal, in quenched and tempered condition. *J–R* curves and crack growth initiation values of fracture mechanics parameter were experimentally and numerically obtained for specimens with a pre-crack in the heat-affected zone (HAZ) and weld metal (WM). The complete Gurson model (CGM) was used in prediction of *J–R* curves and crack growth initiation. It is shown that the resistance to crack initiation and growth can be predicted using micromechanical analysis, and that the results are significantly affected by mechanical heterogeneity of the weldment.

1. Introduction

Crack initiation and stable crack growth in ductile materials are conventionally characterised by fracture resistance curves, obtained from the standard fracture mechanics tests. However, testing of the different specimens often reveals considerable differences in these curves, due to the constraint effects [1–5]. These effects are very important even in homogeneous structures, where the fracture resistance is dependent on geometry of the structure and crack, as well as on the loading type. In welded joints (e.g. specimens notched and pre-cracked in different zones), they are much more pronounced than in homogeneous structures, having in mind the material heterogeneity in addition to the geometry constraints. The service safety of highly loaded welded structures is strongly dependent on the integrity and fracture resistance of their welded joints. Therefore, mechanical heterogeneity of the joint is a key factor for understanding the fracture and failure of such structures under various exploitation conditions [1,2,6,7]. Above-mentioned constraints are the reason why transferring the fracture parameters from specimens to components is especially questionable in case of welded joints. One of the ways to take into account both constraints due to material mismatching and due to geometry is J-Q-M formulation [8–10], derived by extending the J-Q theory [11] of the two-parameter fracture mechanics.

Recently produced high-strength low-alloyed (HSLA) steel, examined in this study as the base metal (BM), typically exhibits large-scale deformation and plastic straining during tearing, which helps to prevent rapid unstable fracture. Such strain state (large scale yielding) is another reason why traditional *J* integral approach of classical fracture mechanics cannot give adequate results [12]. Having in mind all the mentioned issues, micromechanical analysis is used in this work to eliminate or decrease the dependence of fracture parameters on geometry of the structure and material heterogeneity. This approach is chosen as appropriate for fracture assessment, since it correlates the local stresses and strains with resistance to crack initiation and growth. Therefore, the constraint effects are inherent in the analysis, which is not the case in the two-parameter fracture mechanics.

In case the crack is located in the middle of the weld metal (WM), not in the vicinity of the heat affected zone (HAZ), the joint can be analysed as bimaterial, as shown through several studies [1,13–16]. However, there are situations when it is also very important to understand the behaviour of HAZ during the fracture process [17–21], bearing in mind that it is often susceptible to cracks and its toughness may influence the overall fracture behaviour of a welded joint. In [17], experimental tests and FEM analyses have been performed on high strength steel weldments produced

* Corresponding author. Tel.: +381 11 3302 346; fax: +381 11 3370 364.
E-mail address: asedmak@mas.bg.ac.rs (A. Sedmak).

0261-3069/$ - see front matter © 2012 Elsevier Ltd. All rights reserved.
doi:10.1016/j.matdes.2012.01.001

Nomenclature

a	crack length (mm)
a_0	initial crack length (mm)
Δa	crack length increment (mm)
A	strain controlled nucleation rate (–)
A_A	area fraction of inclusions (–)
A_i	area of detected inclusions (mm^2)
A_T	measurement field area (mm^2)
B	specimen thickness (mm)
CMOD	crack mouth opening displacement (mm)
$CTOD_i$	crack tip opening displacement at crack initiation (mm)
E	Young's modulus (GPa)
f	current void volume fraction (–)
f^*	modified void volume fraction (damage function) (–)
f_0	initial void volume fraction (–)
f_c	critical void volume fraction (–)
f_F	void volume fraction at final failure (–)
f_N	volume fraction of void nucleating particles (–)
f_u^*	ultimate void volume fraction (–)
f_v	volume fraction of non-metallic inclusions (–)
$\dot{f}_{growth}$	void volume fraction growth rate (s^{-1})
$\dot{f}_{nucleation}$	void volume fraction nucleation rate (s^{-1})
F	applied force (kN)
J	J-integral (N/mm)
J_i	J-integral at crack initiation (N/mm)
$J_{0.2/BL}$	J-integral at 0.2 mm crack growth offset to the blunting line (N/mm)
n	strain hardening exponent (–)
q_1, q_2	fitting parameters of the Gurson-Tvergaard-Needleman yield criterion (–)
r	void space ratio (–)
S	distance between the support cylinders (mm)
S_{ij}	deviatoric components of the Cauchy stress tensor (MPa)
S_N	standard deviation in the Gaussian distribution of nucleation rate (–)
V_V	volume fraction of detected inclusions (–)
$\bar{V}_V$	mean value of the volume fraction (–)
W	specimen width (mm)

Greek symbols

$\dot{\varepsilon}_{ij}^p$	component of the plastic strain rate tensor (s^{-1})
ε_{eq}^p	equivalent plastic strain (–)
$\dot{\varepsilon}_{eq}^p$	equivalent plastic strain rate (s^{-1})
ε_1, ε_2, ε_3	principal strains (–)
ε_N	mean nucleating strain (–)
φ	yield function of the Gurson–Tvergaard–Needleman model (–)
λ	mean free path between non-metallic inclusions (μm)
ν	Poisson's ratio (–)
σ_1	maximum principal stress (MPa)
σ_m	mean stress (MPa)
σ	current flow stress of the matrix material (MPa)
σ_{eq}	von Mises equivalent stress (MPa)

using two different consumables for different mismatch levels. Almost all fracture initiation points were in the HAZ, and the probability for initiation in the base material and the weld metal was found to be rather small. Welded HSLA steel specimens with a pre-crack in the heat affected zone were examined in [18], and it is shown that the strength mismatching of the homogeneous and heterogeneous joints caused a redirection of the crack propagation towards the low-strength region of the joint. In [19], two HSLA steels of different strength level were welded using the same consumables. Fracture deviation from HAZ into weld or base metal occurred: for the BM with higher strength, the crack propagated from HAZ to WM, while for the BM with lower strength the crack propagated from HAZ to BM. Numerical and experimental investigation of ductile tearing of the welded joint with a pre-crack in HAZ using local approach to fracture is conducted in [20]. The fracture assessment has been done using uncoupled and coupled approach, and special attention has been given to modelling of the crack growth direction (the crack deviated towards the BM).

Besides the cracks initiated in HAZ (e.g. around some initial defect), it is important to take into account the possibility that the fracture path can run through HAZ even if the crack was initiated in WM or BM. Therefore, there are many cases when a welded joint should not be considered as bimaterial. In this work, the crack initiation and propagation is analysed in welded single edge notched bend (SENB) specimens with a pre-crack in WM or HAZ. The aim was to determine the mechanical heterogeneity effect on ductile crack initiation and propagation in high strength steel weldments using the same specimen geometry and loading conditions.

The complete Gurson model (CGM) [22] is applied for ductile fracture modelling. It includes the void coalescence criterion proposed by Thomason [23], and critical damage parameter value (used as failure criterion) is not a material constant, but depends on the stress and strain state in the structure. This fact is especially important in the examined joints, where the material heterogeneity causes severe gradients in the stress and strain fields around the crack tip before and after the crack growth initiation.

2. The complete Gurson model (CGM)

Several micromechanical models have been developed for modelling the behaviour of ductile materials. Among them, the model proposed by Gurson [24] is a widely used one for ductile porous materials. The yield function of Gurson, modified by Tvergaard [25] and Tvergaard and Needleman [26], is used to describe the growth of voids in the material and subsequent macroscopic softening. The modified yield function is defined by the formula:

$$\phi(\sigma_{eq},\sigma_m,\sigma,f) = \left(\frac{\sigma_{eq}}{\sigma}\right)^2 + 2q_1 f^* \cosh\left(\frac{3q_2\sigma_m}{2\sigma}\right)^2 - \left(1+(q_1 f^*)^2\right) = 0 \quad (1)$$

where σ_m is the mean stress, σ is the flow stress of the matrix material, f^* is the modified void volume fraction, and σ_{eq} is the von Mises equivalent stress:

$$\sigma_{eq} = \sqrt{\frac{3}{2}S_{ij}S_{ij}} \quad (2)$$

where S_{ij} stands for the deviatoric components of the stress tensor.

The constants q_1 and q_2 are fitting parameters introduced by Tvergaard [25], to improve the ductile fracture prediction of the Gurson model.

The modified void volume fraction, f^*, often called the damage function [26], is given by:

$$f^* = \begin{cases} f & \text{for} \quad f \leqslant f_c \\ f_c + \frac{f_u^* - f_c}{f_F - f_c}(f - f_c) & \text{for} \quad f > f_c \end{cases} \quad (3)$$

where f_c is the critical void volume fraction at the onset of void coalescence, $f_u^* = 1/q_1$ is the ultimate void volume fraction, and f_F is the void volume fraction at final failure.

The increase in the void volume fraction, f, during an increment of deformation is partly due to the growth of existing voids and partly due to the nucleation of new voids. Thus, the evolution law for the void volume fraction is given in the form:

$$\dot{f} = \dot{f}_{\text{nucleation}} + \dot{f}_{\text{growth}} \tag{4}$$

Nucleation is considered to depend exclusively on the plastic strain in the material and can be estimated by following equation:

$$\dot{f}_{\text{nucleation}} = A\dot{\varepsilon}^p_{\text{eq}} \tag{5}$$

where $\dot{\varepsilon}^p_{\text{eq}}$ is the equivalent plastic strain rate; parameter A is the void nucleation rate, in this work estimated by the following expression [27]:

$$A = \frac{f_N}{S_N\sqrt{2\pi}} \exp\left[-\frac{1}{2}\left(\frac{\varepsilon^p_{\text{eq}} - \varepsilon_N}{S_N}\right)^2\right] \tag{6}$$

f_N is the volume fraction of void nucleating particles, ε_N is the mean strain for void nucleation and S_N is the corresponding standard deviation.

The void volume fraction due to the growth of voids can be estimated by:

$$\dot{f}_{\text{growth}} = (1-f)\dot{\varepsilon}^p_{\text{ij}} \tag{7}$$

where $\dot{\varepsilon}^p_{\text{ij}}$ are diagonal components of the plastic part of the strain rate tensor.

The critical void volume fraction, f_c, is not considered as a material constant in the complete Gurson model. It is determined by Thomason's plastic limit-load criterion [23], with the assumption that all voids remain spherical during the increase of loading. The CGM predicts the onset of coalescence when the following condition is satisfied [22]:

$$\frac{\sigma_1}{\sigma} \geqslant \left(\alpha\left(\frac{1}{r} - 1\right)^2 + \frac{\beta}{\sqrt{r}}\right)(1 - \pi r^2) \tag{8}$$

where $\alpha = 0.1$ and $\beta = 1.2$ are two constants fitted by Thomason. Zhang et al. proposed a linear dependence of α on hardening exponent n for elastic–plastic materials that exhibit strain hardening. σ_1 is the maximum principal stress and r is the void space ratio given by the formula:

$$r = \sqrt[3]{\frac{3f}{4\pi}e^{\varepsilon_1+\varepsilon_2+\varepsilon_3}} \Big/ \left(\frac{\sqrt{e^{\varepsilon_2+\varepsilon_3}}}{2}\right) \tag{9}$$

where ε_1, ε_2 and ε_3 are the principal strains.

3. Materials and experimental procedure

The material studied in this work was HSLA steel, NIOMOL 490 K, which is used as the base metal. Shielded metal arc welding process (SMAW) was performed with consumable VAC 60Ni to weld a plate (300 × 300 × 16 mm). A mixture of shielding gases; 3.8% CO_2 + 93.7% Ar + 2.5% O_2, was used in order to get acicular ferrite, which raises the toughness of the welded joint. The specimens were cut transversely from the welded plate. The shape of welded joint was K, which was selected for the research purpose to make easier positioning of a crack in HAZ. The chemical compositions of the base metal and consumable are listed in Table 1.

Table 1
Chemical composition of base metal, NIOMOL 490 K and consumable in wt.%.

Material	C	Si	Mn	P	S	Mo	Cr	Ni
NIOMOL 490 K	0.123	0.33	0.56	0.003	0.002	0.34	0.57	0.13
VAC 60 Ni	0.096	0.58	1.24	0.013	0.160	0.02	0.07	0.03

Precise estimation of true stress – true strain curves for different welded joint regions is difficult due to the heterogeneous metallurgical and mechanical properties of the joint zones, especially for heat affected subzones. Therefore, they were obtained by testing a smooth tensile plate at room temperature (Fig. 1). The strains were monitored by ARAMIS stereometric measuring system (www.gom.com) for specific area on the specimen, which included the welded joint regions (Fig. 2). The smooth tensile panel was numerically modelled to estimate true stress – true strain curves for all regions of welded joint (base metal BM, coarse grain heat-affected zone CGHAZ, fine grain heat-affected zone FGHAZ and weld metal WM). Numerical strains were compared with experimentally measured ones for different regions of the joint. Iteration procedure was performed by varying yield strength and hardening exponent up to obtaining a good combination, which matches numerical strains with experimental ones (Fig. 3). Fig. 3 shows the heterogeneity effect on strains in all regions of welded joint. It is obvious that the welded joint exhibits slight strength overmatching, and the average strain in HAZ changes rapidly in comparison with BM and WM. First iteration of true stress – true strain curves was chosen as the first estimated curves from experimental results. Large values of true stress – true strain curves beyond ultimate load were extrapolated by fitting the data up to the ultimate stress with calculated true fracture stress and strain. The estimated mechanical properties are given in Table 2 for BM, CGHAZ, FGHAZ and WM.

Quantitative microstructural analysis was performed to estimate the micromechanical parameters: volume fraction (f_v) and mean free path (λ) between the non-metallic inclusions for the zones of the welded joint, according to [28] (Table 3). In the initial stage of ductile fracture of steel, the voids nucleate mostly around non-metallic inclusions. Hence, the initial porosity f_0 is here assumed to be equal to the volume fraction of non-metallic inclusions (f_v). Fig. 4 shows two measurement fields in the weld metal. A group of oxides and sulphides can be seen in the two measurement fields, which are marked by arrows.

Volume fraction of sulphides and oxides in tested steel has been determined on basis of equality with surface fraction [28]:

$$V_v = A_A = \frac{A_i}{A_T} \tag{10}$$

where V_V and A_A are the volume and surface fraction of detected sulphides and oxides respectively, A_i is the area of the detected inclusions and A_T is the measurement field area.

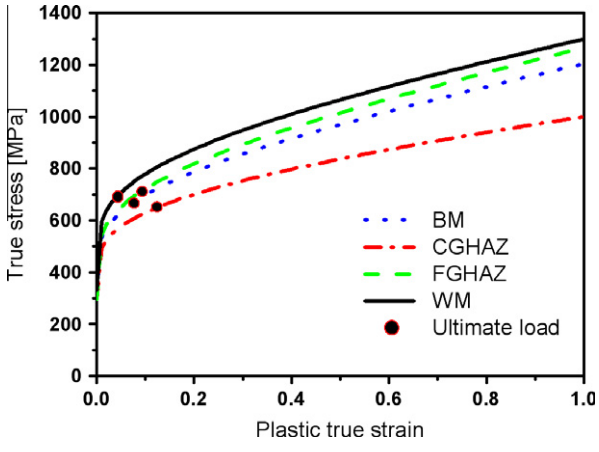

Fig. 1. True stress – true plastic strain curves.

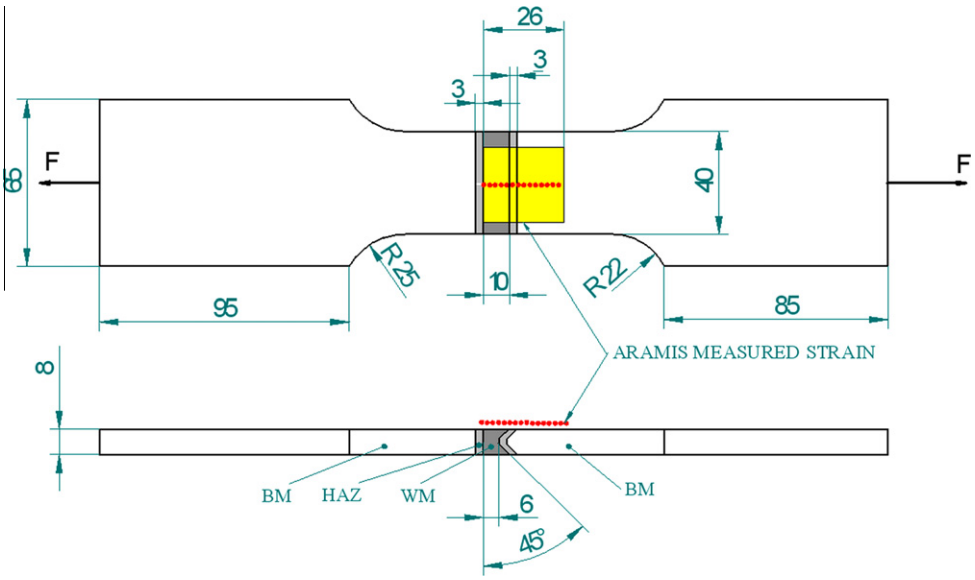

Fig. 2. Geometry of smooth tensile specimen.

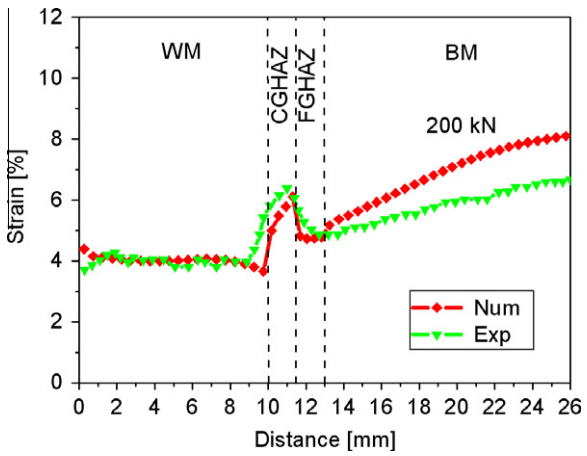

Fig. 3. Comparison between numerical and experimental strain distribution at ultimate load 200 kN.

Table 2
Mechanical properties of the materials.

Material	Young modulus, E (GPa)	Yield strength, σ_Y (MPa)
BM	202.9	520
CGHAZ	203	550
FGHAZ	195	500
WM	200	530

Table 3
Microstructural parameters of the materials.

Material	f_v	f_N	λ (μm)
BM (NIOMOL 490 K)	0.0094	0.014748	578
HAZ	0.0086	0.014748	497
WM	0.0194	0.010685	202

f_v is determined as the mean value of surface fraction of non-metallic inclusions for all measurement fields:

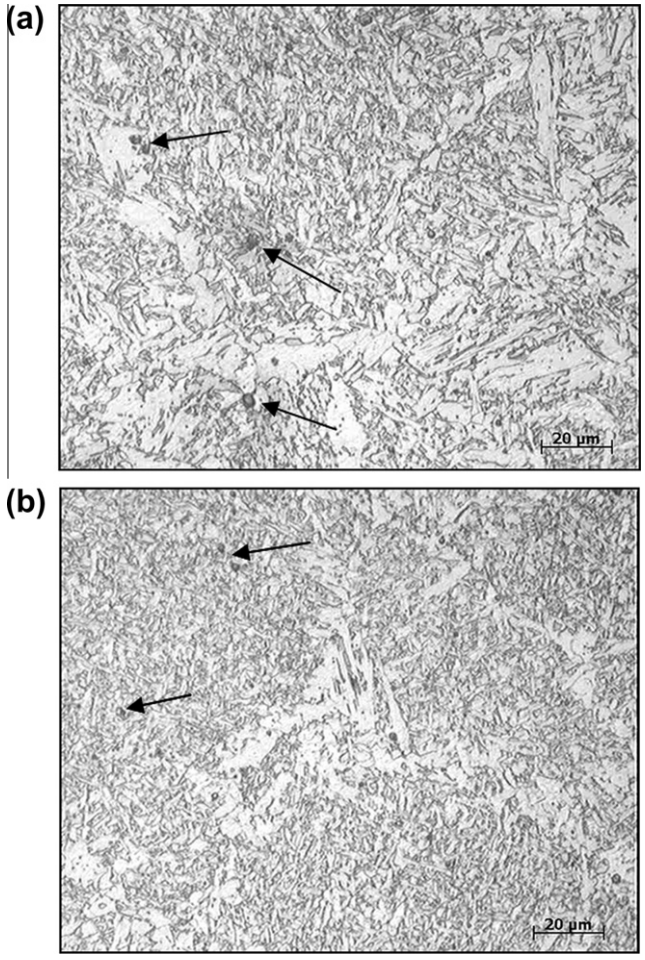

Fig. 4. Two optical micrographs of non-metallic inclusions in the weld metal.

$$f_v = \bar{V}_V = \frac{\sum V_{Vi}}{n} \tag{11}$$

where n is the number of measurement fields.

Volume fraction of secondary void nucleating particles f_N (Table 3; in steel, these are mainly Fe_3C particles), which

represents the effect of secondary voids on ductile fracture, was calculated from the content of carbon in tested materials using the lever rule [29]:

$$\text{wt.\%cem.} = \frac{\%C - 0.025}{6.67 - 0.025} \times 100\% \quad (12)$$

where %C is carbon content in used steel, 6.67 is wt.% of carbon in Fe_3C compound and 0.025 is wt.% of carbon content in ferrite.

Two SENB specimens were used to investigate the fracture behaviour of welded joints: with fatigue pre-cracks in the HAZ and WM. Figs. 5 and 6 show the geometry of both specimens. The initial crack length to specimen width ratio was $a_0/W = 0.49$ and 0.45 for specimens with a pre-crack in WM and HAZ, respectively. The cracks were located in the middle of the weld metal or in the middle of HAZ, between CGHAZ and FGHAZ. Crack growth resistance curves were obtained for both specimens according to the ASTM E1820 standard [30]. The single specimen method was used and the unloading compliance technique was applied for stable crack growth monitoring. Crack mouth opening displacement (CMOD) and applied force (F) were monitored for both specimens.

4. Finite element models

For the determination of the value of stress and strain components and the value of damage parameter (f) in the specimens exposed to external mechanical loading, the FEM software Abaqus (www.simulia.com) was used, with CGM user subroutine, UMAT, developed by Zhang based on [22]. To simplify the finite element analysis, materials of all regions of welded joint were assumed to be isotropic. Isoparametric quadrangular finite elements with 2×2 Gauss integration were used. In front of the crack tip, squared finite elements (0.2×0.2 mm for specimen with a pre-crack in WM and 0.5×0.5 mm for specimen with a pre-crack in HAZ) were used. These sizes approximate the value of the mean free path (λ) between non-metallic inclusions in tested materials (see Table 3). Figs. 7 and 8 show finite element meshes used to model the SENB specimens with a pre-crack in WM and HAZ, respectively.

It is well know that ductile tearing of metals occurs by the nucleation, growth and coalescence of microvoids with significant plastic deformation. Therefore, the zone of interest, containing the crack, is modelled by the CGM and the rest of the model is characterised by elastic–plastic behaviour without damage [31]. Based on this fact, ductile fracture was modelled in the current models by introducing a tearing zone surrounding the crack line, where material degradation and separation can occur. This tearing zone is embedded in a continuous elastic–plastic material where only plastic deformation occurs. Thus, tearing zone was considered in WM for the specimen with a pre-crack in WM and in HAZ for the specimen with a pre-crack in HAZ. The loading of both specimens was controlled by prescribed displacements.

In order to apply the CGM to simulate the ductile tearing in SENB specimens with a pre-crack in WM and HAZ, various model parameters must be defined:

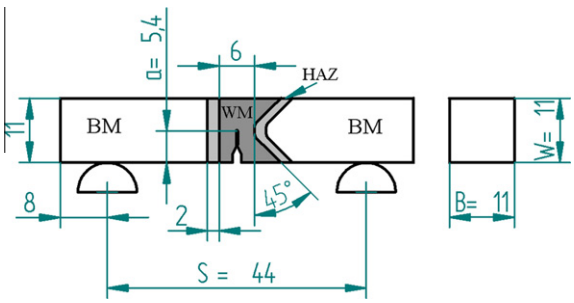

Fig. 5. Geometry of SENB specimen with a pre-crack in WM.

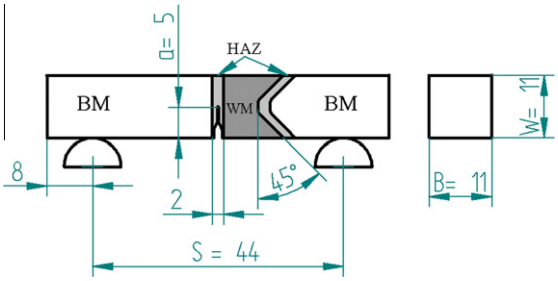

Fig. 6. Geometry of SENB specimen with a pre-crack in HAZ.

The first set of constitutive parameters is q_1 and q_2, which are related to the hardening of the matrix material. In this study, q_1 and q_2 were 1.6 and 1.0, respectively, for SENB specimen with a pre-crack in WM and 1.2 and 1.0, respectively, for SENB specimen with a pre-crack in HAZ. The values of q_1 and q_2 were determined according to the study [32]. The second set of parameters is void initiation and coalescence parameters (f_0, f_c and f_F). Like mentioned previously, the initial void volume fractions (f_0) are assumed to be equal to the volume fractions of non-metallic inclusions (f_v), which is given in Table 3 for BM, HAZ and WM. The critical void volume fraction (f_c) is crucial damage parameter in CGM, since it represents the end of stable void growth and the start of void coalescence. It is not a material constant according to CGM, but it is calculated during the processing procedure, based on the stress and strain fields, see Eq. (9). Void volume fraction at final fracture (f_F) is determined according to the relation $f_F = 0.15 + f_0$ [22]. The third set of parameters (ε_N, S_N, and f_N) is related to secondary voids nucleation. The volume fraction of void nucleating particles (f_N) has been evaluated from Fe_3C content in materials. The nucleation parameters defined by Chu and Needleman, $\varepsilon_N = 0.3$ and $S_N = 0.1$ [27,33,34], were considered for the analysis.

5. Results and discussion

The onset of crack growth and crack resistance curves in analysed welded joints are successfully predicted by using the CGM model. To analyse the transferability of the numerical results and validate the ductile failure model implemented, the numerical and experimental results have to be compared. Figs. 9 and 10 show the comparison between numerical (using the CGM and von Mises yield criterion without damage model) and experimental results of force (F) vs. crack mouth opening displacement (CMOD) for SENB specimens with a pre-crack in WM and HAZ, respectively. A good agreement between the CGM results and experimental ones has been achieved. The damage model (CGM) predicts the load drop after maximum load, which represents the stage of ductile tearing, quite well, whereas the simulation without the damage model cannot predict this phenomenon. It can also be noticed that both specimens have exhibited significant nonlinear behaviour preceding unstable fracture, as expected. This confirms the ductility of materials, which is higher in the HAZ than in the WM. Nevertheless, the differences in the maximal force arise from the weldment mechanical heterogeneity. Moreover, the rate of load drop of the SENB specimen with a pre-crack in the WM is higher than the one of the SENB specimen with a pre-crack in the HAZ. It can be attributed to the effect of volume fraction of non-metallic inclusions, which is higher in WM than in HAZ.

5.1. Numerical modelling of crack initiation

Crack initiation can be predicted by using the CGM model; failure is defined by the instant when the first element in front of the

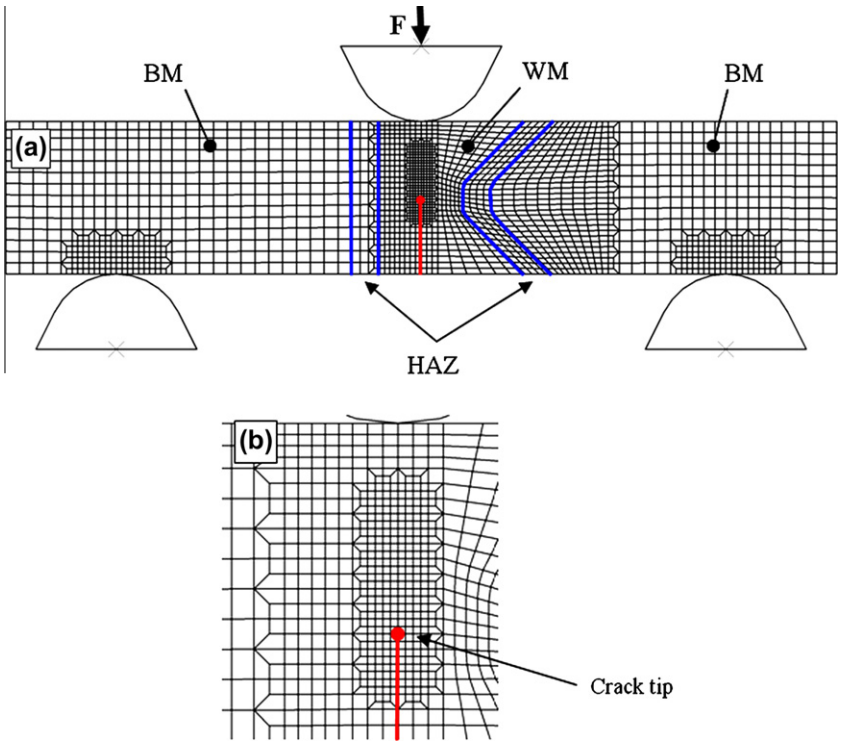

Fig. 7. Finite element mesh of SENB specimen with a pre-crack in WM (a) and detailed crack-tip mesh (b).

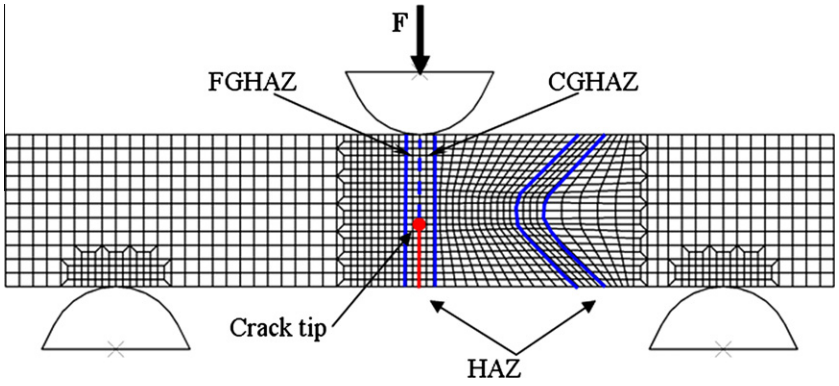

Fig. 8. Finite element mesh of SENB specimen with a pre-crack in HAZ.

crack tip becomes damaged. The condition for the onset of the crack growth (as determined by the J-integral, J_i, or crack tip opening displacement, $CTOD_i$) is most adequately defined by the micromechanical criterion:

$$f \geqslant f_c \tag{13}$$

When the condition given by Eq. (13) is satisfied, the onset of the crack growth occurs. The critical void volume fraction (f_c) in the CGM is determined by evaluating Eq. (8) at the end of each increment step. Once Eq. (8) is satisfied, void coalescence starts and the current void volume fraction is regarded as f_c for that Gauss point. To determine numerically the crack initiation, the increase of void volume fraction (f) is monitored at the Gauss point nearest to the crack tip [35]. When current monitored f reaches f_c and Eq. (13) is satisfied, the fracture mechanics parameter at crack initiation (J_i or $CTOD_i$) is determined.

Crack initiation values for SENB specimens with a pre-crack in WM and HAZ have been determined. In Fig. 11, the increase of the value of f is given as a function of the J-integral for SENB specimens with a pre-crack in WM and HAZ. The J-integral for a stationary crack under loading is obtained by using the domain integral method. It can be noticed in the Fig. 11, the more rapid increase of the void volume fraction (f) was obtained for the specimen with a pre-crack in WM. This can be explained as the effect of mechanical heterogeneity and volume fraction of non-metallic inclusions on the damage f. Distributions of void volume fraction (f) at the crack growth initiation are shown in Fig. 12 for both specimens; concentration of large values very close to the crack tip is obvious. The values of J_i are given in Table 4 with experimentally determined fracture toughness ($J_{0.2/BL}$) using SENB specimens with a pre-crack in WM and HAZ. It is important to know that the value of J_i can be determined experimentally by measuring the stretch zone width according to the ESIS P2-92 procedure [36], while $J_{0.2/BL}$ was determined without measuring the stretch zone width according to ASTM E1820 [30]. The value of $J_{0.2/BL}$ is greater than J_i for the majority of structural materials. The effect of heterogeneity can also be

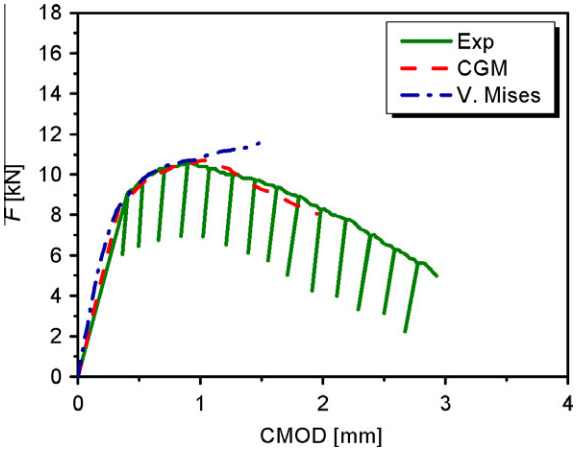

Fig. 9. Force (F) vs. CMOD for SENB specimen with a pre-crack in WM.

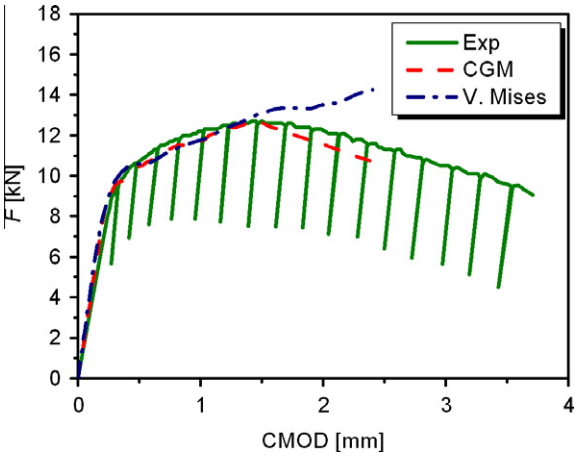

Fig. 10. Force (F) vs. CMOD for SENB specimen with a pre-crack in HAZ.

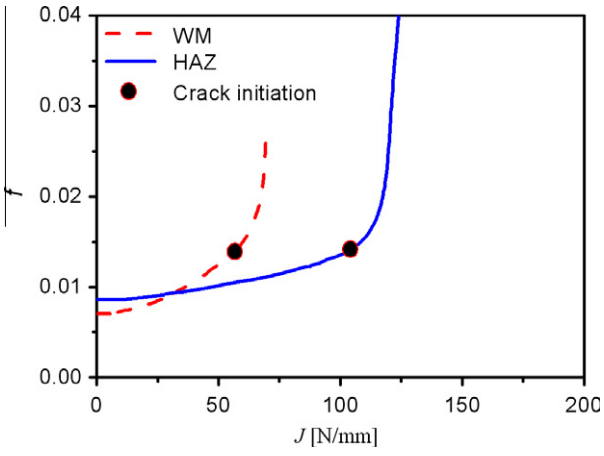

Fig. 11. Void volume fraction (f) vs. J-integral for SENB specimens with a pre-crack in WM and HAZ.

seen on the obtained different values of the J-integral corresponding to the initiation (J_i) of crack growth (Table 4). It can be seen that the value of J_i is larger than the value of $J_{0.2/BL}$ for HAZ, while it is not in the case of WM.

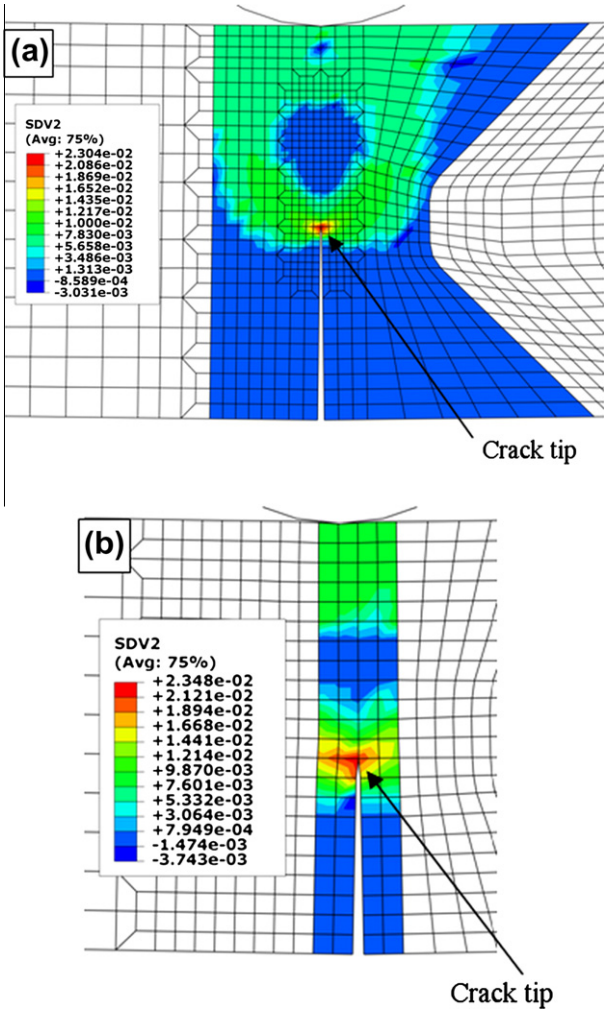

Fig. 12. Distribution of void volume fraction at the crack growth initiation for SENB specimen with a pre-crack in WM (a) and HAZ (b).

Table 4
Experimental ($J_{0.2/BL}$) and numerical (J_i) values for the specimens with a pre-crack in WM and HAZ.

Material	$J_{0.2/BL}$ (N/mm)	J_i (N/mm)
WM	64.7	57.6
HAZ	84	104

5.2. Numerical modelling of crack propagation

Ductile fracture propagation can be simulated by different techniques, including: element splitting, node releasing, element deleting and stiffness decreasing. The last technique has been used in this work.

The computational simulation within an element follows Eq. (3) after it reaches the critical damage value f_c, and continues until the void volume fraction f^*, reaches its maximum value f_u^*. At this point in the simulation, the element is fully failed according to the GTN yield function (Eq. (1)), leading to local stiffness reduction.

J–R curves have been obtained by using specimens with a pre-crack in WM and HAZ. The FE meshes for both specimens are shown in Figs. 7 and 8. In the model of tearing zone, minimum two layers of elements with a highly refined mesh stretch out across the ligament ahead of the crack tip because of expected damage and crack propagation in this region. However, several

researchers [37,38] have introduced a single layer of elements in front of the prospective crack plane to simulate the ductile tearing.

The crack growth (Δa) has been simulated by tracing the path of completely damaged elements, which appear in different colour in Fig. 13. In other words, the crack growth has been estimated by multiplying the original length of an element with the number of damaged elements. The element is assumed to be failed (completely lost its load carrying capacity) when the void volume fraction at final failure (f_F) is reached according to the relation $f_F = 0.15 + f_0$. The crack growth resistance curves were obtained and presented in Figs. 14 and 15 for the cracks in WM and HAZ. It can be seen that good agreement is obtained between experimental and numerical results. It is also obvious that the crack resistance curve of the SENB specimen with a pre-crack in HAZ is higher than the one of the specimen with a pre-crack in WM due to the effect of heterogeneity and slight effect of crack depth. Better fracture resistance of HAZ in comparison with WM, in welded joints produced of HSLA steels of different strength level, has also been obtained in [19]. However, direct comparison with the literature results is very difficult; bearing in mind the possible difference in the base metal and welding consumables manufactured by different producers. Further, even for the exactly same BM and consumable, fracture behaviour of welded joint can depend on welding technology and conditions.

5.3. The influence of FE size on crack initiation and propagation

Several researches analysed the effect of finite element size on the prediction of crack initiation and crack resistance curves [13,14,20,22,31,37,39]. In this study, it is also found that the size of FE mesh significantly affects the material resistance curves and crack initiation values for specimens with a crack in WM and HAZ. The results are in agreement with the literature findings; as the FE size is increased, the fracture toughness also increases, both for crack initiation and crack growth. For both materials, the initial FE size is set to the approximate value of the mean free path (λ) between non-metallic inclusions. In addition, one more mesh size was considered for each specimen; these sizes were chosen as follows: elements larger than λ for WM and elements smaller than λ for HAZ. In this way, two similar finite element sizes are used for each of the materials. Significant effect of FE mesh size on material resistance curves can be seen in Figs. 14 and 15; the best agreement is obtained for the size of the element approximating the mean free path between the non-metallic inclusions λ in analysed materials, given in Table 3. The connection of the FE size and material microstructure (expressed through λ) was confirmed through many studies, including [13,14,34,37]. In some of them, the ratio of the two values is equal to 1, as presented here. This ratio can be different, but the important conclusion is that these quantities are related, which means that FE size (as numerical parameter) depends on λ (as microstructural parameter) and can be regarded as material parameter in the Gurson model.

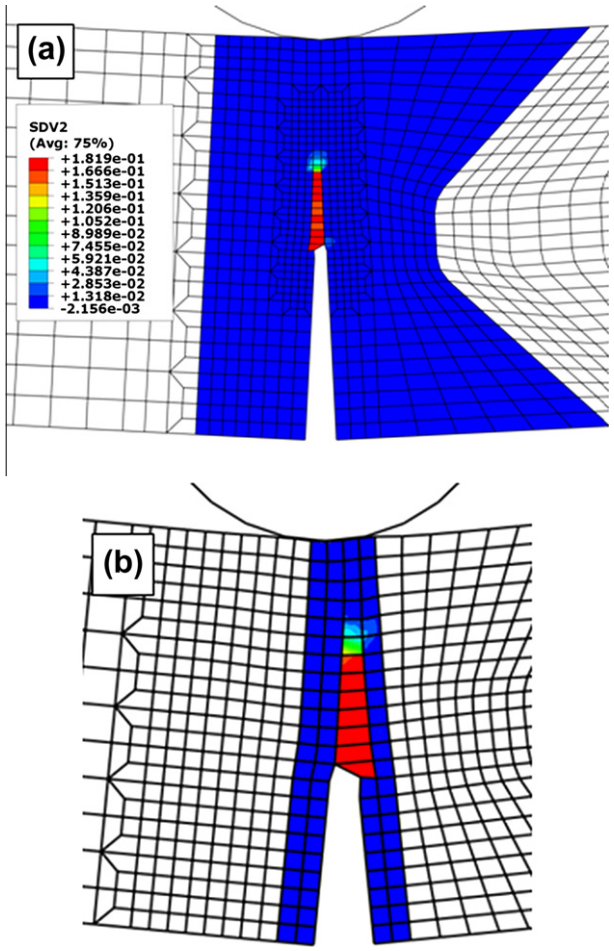

Fig. 13. Distribution of void volume fraction for SENB specimen with a pre-crack in WM (a) and HAZ (b).

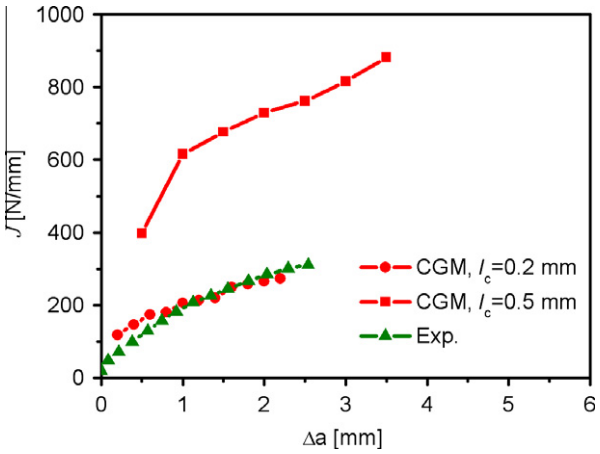

Fig. 14. *J–R* curve for SENB specimen with a pre-crack in WM with the effect of mesh size.

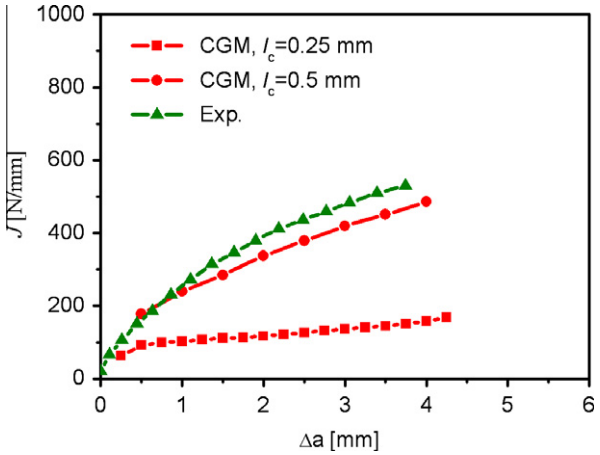

Fig. 15. *J–R* curve for SENB specimen with a pre-crack in HAZ with the effect of mesh size.

6. Conclusion

Mechanical heterogeneity effect on ductile crack initiation and propagation in welded SENB specimens with a pre-crack in HAZ and WM has been analysed in this paper using the complete Gurson model (CGM).

The increasing rate of damage growth ahead of the crack tip in the SENB specimen is smaller in the HAZ than in the WM. This difference can be attributed to much higher initial void volume fraction of the latter, as well as to slightly longer crack in this zone. Crack resistance curves (J–R curves) and crack initiation values were successfully predicted using the CGM and true stress – true strain curves of the welded joint zones. These curves were determined by a combined experimental–numerical procedure, utilising stereometric strain measurement and finite element modelling of smooth tensile panel.

It is shown that the resistance to crack initiation and growth is greatly affected by the heterogeneity of the weldment. The heterogeneity of the examined joints cannot be adequately represented by the often used ratio of the yield strengths, because hardening behaviour and microstructure also influence the fracture behaviour. The yield strengths of the joint zones are similar (less than 10% difference), while fracture resistance exhibits significant differences. The value of the J integral at crack initiation J_i, obtained by the CGM, is larger than the value of J integral for 0.2 mm crack growth $J_{0.2/BL}$ for HAZ, and smaller in the case of WM.

The influence of the finite element size on the results was also analysed. It is found that finite element size near the crack tip strongly influences the prediction of crack initiation and growth, and that there is a very significant difference in appropriate FE size between the WM and HAZ. For the analysed materials, this size corresponds to the mean free path between the non-metallic inclusions in the examined welded joint zones.

Acknowledgements

AS, MR, BM and MZ acknowledge the support from the Serbian Ministry of Science under the projects ON 174004 and E!5348. Authors would also like to thank Z.L. Zhang for the CGM user subroutine.

References

[1] Schwalbe KH, Ainsworth RA, Eripret C, Franco C, Gilles P, Koçak M, et al. Common views on the effects of yield strength mis-match on testing and structural assessment. In: Mis-matching of Interfaces and Welds, GKSS Research Center, Geesthacht; 1997. p. 99–132.
[2] Koçak M, editor. Weld mis-match effect. International Institute of Welding (IIW), IIW Document; 1998. X:1419-98.
[3] Clausmeyer H, Kussmaul K, Roos E. Influence of stress state on the failure behaviour of cracked components made of steel. ASTM Appl Mech Rev 1991;44:77–92.
[4] Hackett EM, Schwalbe K-H, Dodds RH, editors. Constraint effects in fracture. ASTM STP 1171, ASTM, Philadelphia; 1993.
[5] Kirk M, Bakker A, editors. Constraint effects in fracture – theory and applications, vol. 2. ASTM STP 1244, ASTM, Philadelphia; 1995.
[6] Ravi S, Balasubramanian V, Babu S, Nemat Nasser S. Assessment of some factors influencing the fatigue life of strength mis-matched HSLA steel weldments. Mater Des 2004;25:125–35.
[7] Kozak D, Gubeljak N, Konjatić P, Sertić J. Yield load solutions of heterogeneous welded joints. Int J Pres Ves Pip 2009;86:807–12.
[8] Zhang ZL, Hauge M, Thaulow C. Two-parameter characterization of near-tip stress fields for a bi-material elastic–plastic interface crack. Int J Fract 1996;79:65–83.
[9] Burstow MC, Howard IC, Ainswort RA. The influence of constraint on crack tip stress fields in strength mismatched welded joints. J Mech Phys Solids 1998;46:845–72.
[10] Betegon C, Penuelas I. A constraint based parameter for quantifying the crack tip stress fields in welded joints. Eng Fract Mech 2006;73:1865–77.
[11] O'Dowd NP, Shih CF. Family of crack-tip fields characterized by a triaxiality parameter III. Structure of field. J Mech Phys Solids 1991;39:989–1015.
[12] Schmitt W, Kienzler R. The J-integral concept for elastic–plastic material behaviour. Eng Fract Mech 1989;32:409–18.
[13] Penuelas I, Betegon C, Rodriguez C. A ductile failure model applied to the determination of the fracture toughness of welded joints. Numerical simulation and experimental validation. Eng Fract Mech 2006;73:2756–73.
[14] Rakin M, Gubeljak N, Dobrojevic M, Sedmak A. Modeling of ductile fracture initiation in strength mismatched welded joint. Eng Fract Mech 2008;75:3499–510.
[15] Chhibber R, Biswas P, Arora N, Gupta SR, Dutta BK. Micromechanical modelling of weldments using GTN model. Int J Fract 2011;167:71–82.
[16] Wang T, Yang JG, Liu XS, Dong ZB, Fang HY. Stress intensity factor expression for center-cracked butt joint considering the effect of joint shape. Mater Des 2012;35:72–9.
[17] Moltubakk T, Thaulow C, Zhang ZL. Application of local approach to inhomogeneous welds. Influence of crack position and strength mismatch. Eng Fract Mech 1999;62:445–62.
[18] Gubeljak N. Fracture behaviour of specimens with surface notch tip in the heat affected zone (HAZ) of strength mis-matched welded joints. Int J Fract 1999;100:155–67.
[19] Rak I, Treiber A. Fracture behaviour of welded joints fabricated in HSLA steels of different strength level. Eng Fract Mech 1999;64:401–15.
[20] Wilsius J, Imad A, Nait Abdelaziz M, Mesmacque G, Eripret C. Void growth and damage models for predicting ductile fracture in welds. Fatigue Fract Eng Mater Struct 2006;23:105–12.
[21] Toyoda M, Minami F, Ruggieri C, Thaulow C, Hauge M. Strength mis-match effect on fracture behaviour of HAZ. In: Mis-matching of Interfaces and Welds, GKSS Research Center, Geesthacht; 1997. p. 75–98.
[22] Zhang ZL, Thaulow C, Odegard J. A complete Gurson model approach for ductile fracture. Eng Fract Mech 2000;67:155–68.
[23] Thomason PF. Ductile fracture of metals. Oxford: Pergamon Press; 1990.
[24] Gurson Al. Continuum theory of ductile rupture by void nucleation and growth, part I. Yield criteria and flow rules for porous ductile media. J Eng Mater Technol 1977;99:2–15.
[25] Tvergaard V. Influence of voids on shear bands instabilities under plane strain conditions. Int J Fract 1981;17:389–407.
[26] Tvergaard V, Needleman A. Analysis of cup-cone fracture in a round tensile bar. Acta Metall 1984;32:157–69.
[27] Chu C, Needlman A. Void nucleation effects in biaxiality stretched sheets. ASME J Eng Mater Technol 1980;102:249–56.
[28] ASTM E1245-89. Standard practice for determining inclusion content of steel and other metals by automatic image analysis. Philadelphia: American Society for Testing and Materials; 1989.
[29] Awerbuch J. Fundamentals of mechanical behavior of materials. Philadelphia: Wiley Custom Publishing; 2001.
[30] ASTM E1820-08. Standard test method for measurement of fracture toughness. Philadelphia: American Society for Testing and Materials; 2008.
[31] Chen Y, Lambert S. Analysis of ductile tearing of pipeline-steel in single edge notch tension specimens. Int J Fract 2003;124:179–99.
[32] Faleskog J, Gao X, Shih CF. Cell model for nonlinear fracture analysis-I. Micromechanics calibration. Int J Fract 1998;89:365–73.
[33] Betegon C, Rodriguez C, Belzunce FJ. Analysis and modelisation of short crack growth by ductile fracture micromechanisms. Fatigue Fract Eng Mater Struct 1997;20:633–44.
[34] Dutta BK, Guin S, Sahu MK, Samal MK. A phenomenological form of the q_2 parameter in the Gurson model. Int J Pres Ves Pip 2008;85:199–210.
[35] Rakin M, Cvijovic Z, Grabulov V, Putic S, Sedmak A. Prediction on ductile fracture initiation using micromechanical analysis. Eng Fract Mech 2004;71:813–27.
[36] ESIS P2-92. Procedure for determining the fracture behavior of materials. European Structural Integrity Society: ESIS Publication; 1992.
[37] Ruggieri C, Panontin TL, Dodds RH. Numerical modeling of ductile crack growth in 3-D using computational cell elements. Int J Fract 1996;82:67–95.
[38] Gao X, Faleskog J, Shih F. Cell model for nonlinear fracture analysis-II. Fracture-process calibration and verification. Int J Fract 1998;89:375–89.
[39] Bernauer G, Brocks W. Numerical round robin on micro-mechanical models – Results. ESIS TC8. Geesthacht: GKSS Research Center; 2000.